Journal of Sustainable Metallurgy (2023) 9:1444–1455
https://doi.org/10.1007/s40831-023-00736-8

RESEARCH ARTICLE

Measurement of SnO Activity Coefficient in $CaO–SiO_2–Fe_tO–Al_2O_3$ Slag Saturated with Fe

Yasunari Shinoda[1,4] · Takayuki Iwama[2] · Mizuki Kato[2,5] · Hiromitsu Watanabe[3] · Satoshi Nakagawara[3] · Hiroki Takasu[1] · Yukitaka Kato[1] · Ryo Inoue[2] · Shigeru Ueda[2]

Received: 14 May 2023 / Accepted: 17 August 2023 / Published online: 13 September 2023

Abstract

It is important to clarify the behavior of elements in the reaction between molten $CaO–SiO_2–Fe_tO–Al_2O_3$ slag and liquid metal during the remelting of Cu scrap. To estimate the desirable slag composition for retaining Sn in metal, the effects of the slag basicity and the concentrations of Fe_tO and Al_2O_3 on the SnO activity coefficient were investigated. Molten $CaO–SiO_2–Fe_tO$ slag (with optional Al_2O_3 addition) was reacted with liquid Pb–Sn alloy in a pure Fe crucible at 1573 K for 5 h while blowing the $CO–CO_2$ mixture. From the activity coefficients of Sn, Pb, and Fe oxides in the slag, which were calculated using the P_{CO}/P_{CO2} ratio during heating and the chemically analyzed compositions of slag and metal, their behaviors in slag/metal reaction were discussed. The order of reducibility was $PbO > SnO >> Fe_tO$. Finally, it was suggested from the thermodynamic and industrial smelting perspectives that the slag condition favorable to SnO reduction is high basicity, around 50 mass% Fe_tO, and low Al_2O_3 content.

The contributing editor for this article was Adam Clayton Powell.

✉ Takayuki Iwama
takayuki.iwama.a6@tohoku.ac.jp

Yasunari Shinoda
o109034y@mail.kyutech.jp

Mizuki Kato
mizuki.kato.s7@alumni.tohoku.ac.jp

Hiromitsu Watanabe
watanah2@dowa.co.jp

Satoshi Nakagawara
nakagaws@dowa.co.jp

Hiroki Takasu
takasu.h.aa@m.titech.ac.jp

Yukitaka Kato
kato.y.ae@m.titech.ac.jp

Ryo Inoue
ryo.inoue.e2@tohoku.ac.jp

Shigeru Ueda
shigeru.ueda.a5@tohoku.ac.jp

[1] Laboratory for Zero-Carbon Energy, Institute of Innovative Research, Tokyo Institute of Technology, 2-12-1 Ookayama, Meguro-ku, Tokyo 152-8550, Japan

[2] Institute of Multidisciplinary Research Advanced Material, Tohoku University, 2-1-1 Katahira, Aoba-ku, Sendai 980-8577, Japan

[3] Technical Research Center, Dowa Metals & Mining Co., Ltd., 60-1 Otarube, Kosaka-Machi, Kazuno-Gun, Akita 017-0202, Japan

[4] Wafer Process Engineering Department, Shirakawa Plant, Shin-Etsu Handotai Co., Ltd., 150 Oh-hira, Odakura, Nishigo, Nishi-shirakawa, Fukushima 961-8061, Japan

[5] Steel Production Engineering Department, Aichi Steel Corporation, 1 Wanowari Araomachi, Tokai 476-8666, Japan

Graphical Abstract

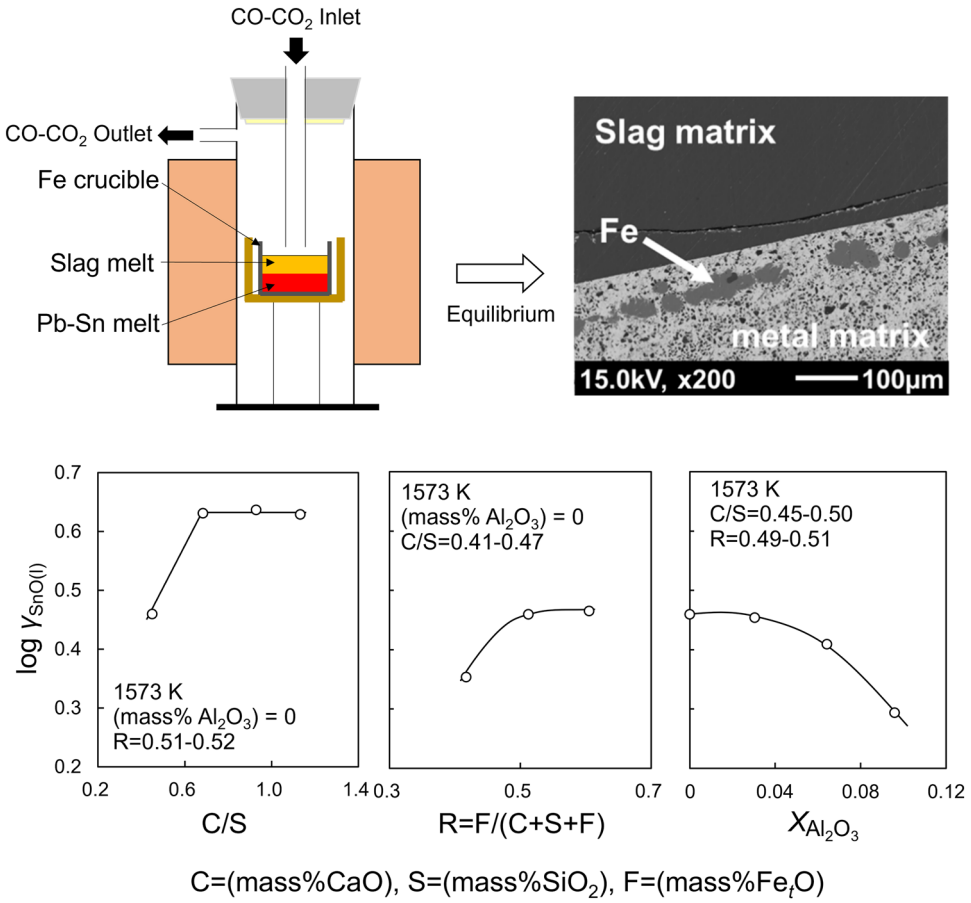

Keywords Sustainability · Recycling · Sn · Activity coefficient · Equilibrium

Introduction

The consumption of metal resources in the world is growing rapidly [1]. In the next few decades, the demand for natural resources is expected to be several times higher than the current reserves [2, 3]. In such global situation, since natural resources are scarce in Japan, Japanese industries have constantly faced supply risks [4–6]. Moreover, since the mining and refining of raw natural resources require a large amount of energy in response to the expansion of those demands, the global environment faces the challenge of massive CO_2 and other greenhouse gas emissions [7, 8]. On the other hand, Japan could have accumulated a large amount of metal resources [9–11]. Those resources, which are present in the form of substrates and household appliances, have the potential to have apparent reserves and higher grades than natural ores [12, 13]. With increasing resource accumulation, which is called an 'urban mine (UM)', the recycling of those resources has come to play a crucial role in the circular economy [3]. It will be advantageous for energy and the economy if spent valuable metals can be recovered efficiently from UM [10, 14]. In addition, the global environment, which is affected by the exploitation of natural resources, can be protected by recovering [15]. Therefore, recovering and recycling of metal elements is a key technology for the construction of a sustainable society. For example, there is a typical high-temperature process where scrap material is melted, oxidized, and reduced to separate metal phase, which contains valuable elements such as gold, silver, lead, and tin [16]. This metal phase is divided into each metallic element by electrorefining and/or multistage extraction [17].

The minable reserve of Sn is so small [18] that Sn is one of the valuable metals whose recovery from scrap materials is being attempted [19]. To recycle Sn from scrap materials, especially Waste from Electrical and Electronic Equipment (WEEE) used mainly as solder, they are fed to copper smelter and then the furnace specialized for

recycling [20, 21]. When recovering Sn by the process, Sn is distributed to Cu-based metal phase and slag phase. In the latter, Sn is dissolved in the form of SnO. For the efficient recovery of Sn in this process, it is required to maximize the Sn distribution to the metal phase. In contrast, Fe, which is an impurity in the metal phase, should be removed by its distribution to the slag phase. When the slag reduction is simply enhanced, FeO is reduced simultaneously with SnO, and the Fe concentration in the metal phase increases [22] and eventually metallic iron is solidified and suspended. This leads to poor fluidity and workability. Therefore, the reduction of only SnO in the slag phase is preferred in practical operation. For this specific reduction, it is necessary to evaluate the optimum conditions concerning slag composition, temperature and oxygen partial pressure by using the activity coefficient of SnO in slag.

Distribution behavior and thermodynamic data of Sn in ordinary Sn and Pb smelting process are well studied [23–30]. In WEEE recycling, CaO–SiO_2–Fe_tO(–Al_2O_3) slag system is applied for operating [31]. Some of researchers have reported a Sn distribution between copper metal and slag and activity coefficient of SnO in the slag. Takeda et al. investigated using the slags saturated with calcium ferrite or iron silicate [32]. Anindya et al. also studied using this slag system under the flow of CO–CO_2 mixture [33]. Nagamori et al. reported the Sn distribution between FeO–Fe_2O_3–SiO_2–Al_2O_3–$CuO_{0.5}$ slag and copper [34]. In all of those studies, slag liquids equilibrated with molten Cu-based metal, and the activity coefficient of SnO was calculated using the data of Sn activity coefficient in Cu metal [35, 36].

To discuss a Sn migration from slag to metal without Fe-oxide reduction, the elucidation of Sn distribution behavior between slag and metal under the saturation of solid Fe is required, because it is the most reducible condition suitable for the deposition of solid Fe. However, there is currently insufficient research investigating the effect of slag composition on Sn distribution under this experimental condition.

Against those backgrounds, this study measured the activity coefficients of SnO and Fe_tO in CaO–SiO_2–Fe_tO(–Al_2O_3) molten slag saturated with solid Fe at 1573 K by equilibrium experiments. Moreover, the activity coefficient PbO was also measured by using Pb–Sn alloy as metal phase, since Pb is contained in WEEE along with Sn and the recovery of Pb is also required. From the results obtained as functions of slag basicity, Fe_tO and alumina concentrations in CaO–SiO_2–Fe_tO slag, and oxygen potentials, the operation condition suitable for reducing SnO and PbO but not FeO was discussed.

Experimental

Slag Preparation

Table 1 shows the target compositions of slag and Pb–Sn alloy used in this equilibrium experiment.

In this table, to simplify the description of the slag compositions, the symbols *C/S* and *RF*, which are defined by Eqs. (1) and (2), respectively, are introduced, referring to a previous report [37].

$$C/S = (\text{mass\% CaO}) / (\text{mass\% SiO}_2) \tag{1}$$

$$RF = (\text{mass\% Fe}_t\text{O}) / \{(\text{mass\% Fe}_t\text{O}) + (\text{mass\% CaO}) + (\text{mass\% SiO}_2)\} \tag{2}$$

herein *C/S* is called 'slag basicity', and *RF* is the Fe_tO mass ratio in CaO–SiO_2–Fe_tO pseudo-ternary system, where (mass% Fe_tO) is the FeO mass concentration calculated assuming that all Fe oxides in slag is present as FeO.

Using the No. 1 sample as the reference, the following three experimental conditions with varying *C/S*, *RF*, and Al_2O_3 concentrations were chosen to achieve

Table 1 Target composition of this study's synthetic slags (mass%) and gas conditions

Sample no	Content in slag (mass%)				*C/S*	*RF*	$P_{O2}\times10^{12}$ (atm)	P_{CO}/P_{CO2}
	CaO	SiO_2	Fe_tO	Al_2O_3				
1	15.5	34.5	50.0	–	0.45	0.50	4.05	6.39
2	21.3	30.4	48.3	–	0.70	0.48	7.03	4.85
3	24.6	27.4	48.0	–	0.90	0.48	11.3	3.82
4	27.1	24.6	48.3	–	1.1	0.48	11.4	3.80
5	18.6	41.4	40.0	–	0.45	0.40	1.84	9.47
6	12.4	27.6	60.0	–	0.45	0.60	6.59	5.01
7	15.3	34.1	45.6	5.0	0.45	0.48	3.71	6.68
8	14.5	32.3	43.2	10.0	0.45	0.48	3.34	7.03
9	13.7	30.5	40.8	15.0	0.45	0.48	2.99	7.44

slag compositions applicable to actual operations. As an actual WEEE recycling slag composition, *C/S*, *RF*, and mass%Al_2O_3 are 0.53, 0.28, and 31.6, respectively [31]. However, depending on adapted process, operability, feed stock, and so on, the contents of CaO, SiO_2, FeO, and Al_2O_3 vary. Therefore, by changing those variables, their effects were evaluated in this study.

(I) The values of *C/S* were changed to 0.45, 0.7, 0.9, and 1.1 with $RF \approx 0.5$ (Nos. 1 to 4). Since *RF* is automatically determined in equilibrium with CO–CO_2 gas, P_{CO}/P_{CO2} ratio was adjusted so that the equilibrium composition became $RF \approx 0.5$.
(II) The values of *RF* were changed from 0.5 (No. 1) to 0.4 and 0.6 (Nos. 5 and 6) with $C/S = 0.45$.
(III) The Al_2O_3 content was increased from 0 mass% (No. 1) to 5, 10, and 15 mass% with $C/S = 0.45$ and $RF \approx 0.5$ (Nos. 7 to 9).

From the phase diagram of the CaO–SiO_2–Fe_tO system [37] and that of the CaO–SiO_2–Al_2O_3 pseudo-ternary system at $RF = 0.5$, which were drawn by the thermodynamic equilibrium calculation software 'FactSage 8.1' [38], all experimental points listed in Table 1 are in the range of liquid phase.

Reagents $CaCO_3$ (99.5% up, FUJIFILM Wako pure chemical), SiO_2 (99.9% up, FUJIFILM Wako pure chemical), FeO (99.5% up, HAYASHI pure chemical), and Al_2O_3 (99% up, KANTO chemical) were applied for slag preparation. In this study, a CaO–SiO_2–Fe_tO master slag was first prepared as follows: $CaCO_3$ and SiO_2 reagents were mixed and pressed to a cylindrical shape by applying a pressure of 2 tons cm^{-2}. Then, the mixture was calcined by holding it in a Pt crucible at 1273 K under an air atmosphere for more than 10 h to remove CO_2 and pre-sinter the mixture of CaO and SiO_2. This pellet was crushed, mixed with FeO, and melted in a Fe crucible at 1573 K under an Ar (G1 grade, TAIYO NIPPON SANSO JFP) atmosphere. By using a Fe crucible during the pre-melting of slag, it is possible to suppress the Fe_2O_3 generation as much as possible due to the Fe/FeO equilibrium. After melting, the crucible was taken out of the furnace, and poured the molten slag onto a stainless steel plate for quenching with He gas blowing. The obtained master slag was crushed to less than 0.1 mm and mixed with SiO_2, FeO, and Al_2O_3 reagents to achieve the respective composition. Finally, the mixture was pressed to a cylindrical shape by applying a pressure of 2 tons cm^{-2}.

Procedure

The CaO–SiO_2–Fe_tO slag containing the respective Al_2O_3 concentration (12 g) was equilibrated with Pb–Sn alloy (18 g), which was prepared by granular Pb (99.5% up, KANTO chemical) and Sn (99.5% up, FUJIFILM Wako pure chemical), in a pure Fe crucible ($\phi 32 \times \phi 27 \times 50$ mm) at 1573 K for 5 h while blowing CO–CO_2 mixed gas (300 mL min^{-1}) on the surface of molten slag. The reason for using Pb–Sn alloy is its low solubility in Fe crucible. Copper alloy and pure Sn cannot be used because they would melt Fe crucible. Furthermore, by using the Pb–Sn alloy, the activity coefficients of SnO and PbO in the slag can be simultaneously measured. This experimental temperature (1573 K) is close to the actual operating conditions and the same as previous research [39]. Kato et al. reported that the equilibrium of Fe crucible/slag melt/Pb melt/CO–CO_2 gas was achieved in 5 h and the change of slag composition was not observed [40]. Based on this report, the holding time at high temperature was determined to be 5 h in this study.

In equilibrium experiments, Fe crucible containing metal and slag was inserted to the soaking zone of a vertical furnace with silicon carbide heating element under an Ar flow (500 mL min^{-1}) using Mo rod. After then, the Ar flow was stopped, and the mixture of CO and CO_2 gases was blown on the surface of molten slag to control the partial oxygen pressure, P_{O2}. The flow rates of CO (G1 grade, TAIYO NIPPON SANSO JFP) and CO_2 (G1 grade, TAIYO NIPPON SANSO JFP) gases were fixed by separate mass flow controllers, which were calibrated with a soap film flow meter. The CO/CO_2 equilibrium and its standard Gibbs free energy, ΔG°, are written by Eqs. (3) and (4), respectively [41].

$$CO(g) + 1/2\ O_2(g) = CO_2(g) \tag{3}$$

$$\Delta G^\circ_{(3)} = -282580 + 86.015\ T\ [\text{Joule}]\ (298 - 3000\ \text{K}) \tag{4}$$

where T is absolute temperature [K]. From Eq. (4), P_{CO}/P_{CO2} ratio is represented by Eq. (5), where P_{CO} and P_{CO2} are CO and CO_2 partial pressure [atm], respectively.

$$\log\left(P_{CO}/P_{CO2}\right) = -14761/T + 4.493 - 1/2 \log P_{O2} \tag{5}$$

The following method was applied to maintain the desired FeO concentration in slag. When the FeO in slag equilibrates with solid Fe according to Eq. (6), the FeO activity, a_{FeO}, is derived from Eqs. (7) and (8) [41].

$$Fe(s) + 1/2\ O_2(g) = FeO(s) \tag{6}$$

$$\Delta G^\circ_{(6)} = -264330 + 64.73\ T\ [\text{Joule}]\ (298 - 1650\ \text{K}) \tag{7}$$

$$= -RT\ln\left\{\left(a_{FeO(s)}\right)/\left(a_{Fe(s)} \cdot P_{O2}^{1/2}\right)\right\} \tag{8}$$

where R is the gas constant [J K^{-1} mol^{-1}]. Since the Fe crucible was used in this experiment, the Fe activity is unity. The FeO activity, $a_{FeO(s)}$, can be expressed by Eq. (9) using

the activity coefficient, $\gamma_{FeO(s)}$, and mole fraction, X_{FeO}, of FeO.

$$a_{FeO(s)} = \gamma_{FeO(s)} \cdot X_{FeO} \quad (9)$$

From Eqs. (7) to (9), the relationship between X_{FeO} and P_{O2} is given by Eq. (10).

$$\log P_{O2} = -27615/T + 6.762 + 2\log\gamma_{FeO(s)} + 2\log X_{FeO} \quad (10)$$

The values of $\gamma_{FeO(s)}$ are evaluated from $\gamma_{FeO(l)}$ reported by Kudo et al. [37], whose standard state was liquid, after converting from liquid to solid using $\Delta G^{\circ}_{(11)}$ [42].

$$FeO(l) = FeO(s) \quad (11)$$

$$\Delta G^{\circ}_{(11)} = -22110 + 13.5T \quad (12)$$

The P_{CO}/P_{CO2} ratio to achieve the desired Fe$_t$O concentration can be estimated by Eqs. (5) and (10). The calculated P_{O2} and P_{CO}/P_{CO2} ratio for each slag sample are also given in Table 1. It is expected that more accurate γ_{FeO} will be obtained in this study.

After 5 h, the Fe crucible was quickly removed from the furnace using Mo rod and immersed in water to cool the sample from the outside of the Fe crucible. Simultaneously, the surface of the slag, which covered metal phase, was cooled by He gas blowing. After confirming a solidification of the slag surface, the Fe crucible was completely immersed in water and rapidly cooled.

After cooling, the Fe crucible was cut vertically along with slag and metal. A cross-sectioned surface of cut piece was mirror-polished and observed by Scanning Electron Microscope and Electron Probe Micro Analyzer (JEOL, JXA-8200) to confirm the absence of the micro metal particles dispersed in slag phase and the micro slag particles in metal phase. From the cross-sectioned sample of another cut piece, approximately 1 g of slag and metal samples were taken for chemical analysis. After dissolving 0.1 g of them with hot 0.2 v/v% HF-mineral acids, the compositions of slag and metal phases were determined using Inductively Coupled Plasma−Atomic Emission Spectroscopy (SPECTRO, ARCOS EOP system). Three to four standard solutions with various concentrations of Sn, Pb, Si, Ca, Fe, and Al were prepared by diluting 1000 mg/L elemental standard solutions [Sn in 3 mol/L HCl, $Pb(NO_3)_2$ in 0.1 mol/L HNO_3, Na_2SiO_3 in 0.2 mol/L Na_2CO_3, $CaCO_3$ in 0.1 mol/L HNO_3, Fe in 0.2 mol/L HNO_3, and Al in 0.2 mol/L HNO_3, FUJIFILM Wako pure chemical].

Results and Discussion

Observation of Samples

The photos of the sample after quenching are shown in Fig. 1. It is found from Fig. 1a that the surface of Pb–Sn alloy in the Fe crucible is covered with the slag layer. In Fig. 1b, the slag phase is observed at the upper part and the metal phase at the lower part. Although Pb and Sn in molten metal are thermodynamically less oxidizable, and the

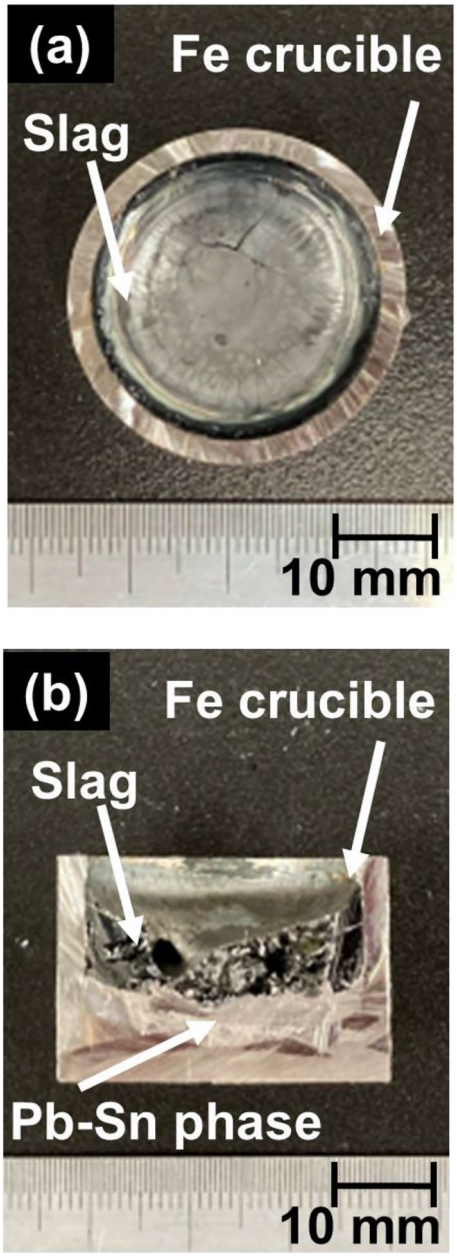

Fig. 1 Photos of the sample after equilibrium experiments: **a** slag surface, **b** cross-section

equilibrium vapor pressures of Pb, Sn and their compounds are higher than iron, it is believed that only a small amount of Pb and Sn evaporated, but enough remained due to slag covering.

Because of the possibility of spinel ($FeAl_2O_4$) formation in sample No. 9, whose Al_2O_3 concentration is highest in the samples given in Table 1, SEM and EPMA observations were made at the area of slag/metal boundary and that away from the boundary. Figure 2a shows an SEM image of the slag phase away from the slag/metal boundary. It is confirmed that there is no spinel formation and undissolved reagents, and the slag phase is homogeneous. No significant particle suspension was also observed in the metal phase. An SEM image near the slag/metal boundary is shown in Fig. 2b. Suspension of fine Fe particles is observed in the metal phase. Fe particles, which are considered to generate by the reaction (13) between Pb metal and FeO in slag, are suspended in the Pb phase near the interface.

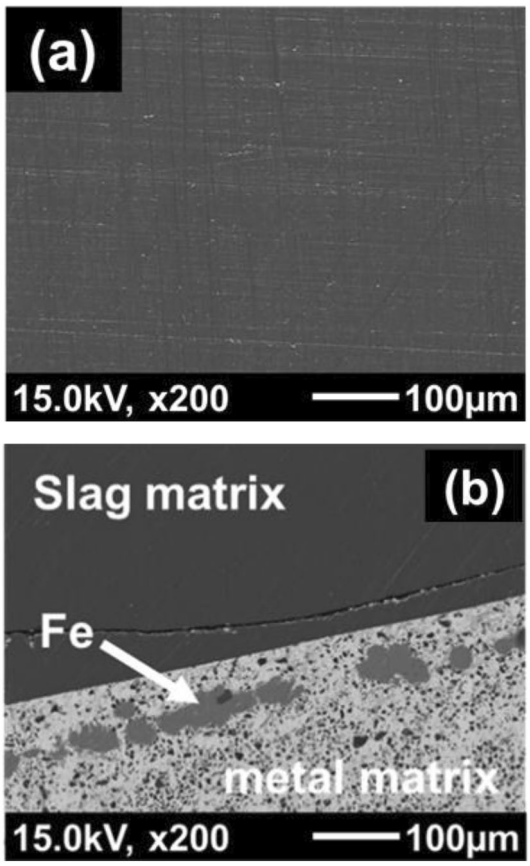

Fig. 2 SEM images of the cross-section of the slag phase away from the slag/metal interface (**a**) and that of the interface (**b**) in sample No. 9

$$Pb(l) + (FeO) = (PbO) + Fe(s) \quad (13)$$

It is suggested that the equilibrium compositions of slag and metal could be obtained by sampling at the areas away from the slag/metal interface.

Activity Coefficients of SnO, PbO, and Fe_tO

The analyzed chemical compositions after equilibrium experiments are listed in Table 2. The same sample solution was measured three times by ICP-AES, and additional sample solutions for Nos. 1, 5, and 9 in Table 2 were prepared and measured. As a result, the analytical errors (relative values) were ± 3% for Sn and Pb and ± 2% for the other elements. The values of *C/S* and *RF* after the equilibrium experiment are only slightly different from those in Table 1. Therefore, it can be said that the P_{CO}/P_{CO2} ratios evaluated from Eqs. (5) and (10) were appropriate, and the equilibrium experiments were performed under the predicted conditions, although Pb, Sn, and their compounds are volatile and susceptible to P_{O2}.

Although the tin oxide in slag is mainly composed of tin monoxide, with a small amount of tin dioxide, it is assumed in this study that all tin oxide is present as SnO [43]. The Sn(l)/SnO(l) equilibrium is written by Eq. (14) [41].

$$Sn(l) + 1/2\ O_2(g) = SnO(l) \quad (14)$$

Table 2 Analyzed chemical compositions of samples after equilibration

Sample No	Content in slag (mass%)						*C/S*	*RF*	Sn in Pb (mass%)
	CaO	SiO_2	Fe_tO	Al_2O_3	SnO	PbO			
1	15.2	33.7	51.4	–	0.28	0.11	0.45	0.51	2.86
2	20.4	29.9	51.7	–	0.26	0.07	0.68	0.51	2.93
3	23.4	25.1	53.0	–	0.33	0.08	0.93	0.52	2.98
4	25.7	22.7	52.1	–	0.33	0.02	1.13	0.52	2.93
5	18.7	39.9	42.0	–	0.26	0.12	0.47	0.42	3.02
6	11.3	27.5	59.6	–	0.33	0.05	0.41	0.61	2.78
7	16.6	33.5	48.2	4.9	0.29	0.22	0.50	0.49	3.01
8	14.4	31.5	45.0	9.9	0.29	0.21	0.46	0.49	2.98
9	13.8	30.2	43.0	14.6	0.32	0.39	0.46	0.49	2.98

$$\Delta G^{\circ}_{(14)} = -258195 + 77.08\,T\ \text{[Joule]}\ (1250 - 1500\ \text{K}) \tag{15}$$

The effective temperature range of $\Delta G^{\circ}_{(14)}$ is 1250–1500 K, but it is assumed in this study that $\Delta G^{\circ}_{(14)}$ can also be valid at 1573 K. The activity of SnO in slag, $a_{\text{SnO(l)}}$, and that of Sn in metal, $a_{\text{Sn(l)}}$, are expressed by Eqs. (16) and (17), respectively, using activity coefficient, γ_i, and mole fraction, X_i, of i.

$$a_{\text{SnO(l)}} = \gamma_{\text{SnO(l)}} \cdot X_{\text{SnO}} \tag{16}$$

$$a_{\text{Sn(l)}} = \gamma_{\text{Sn(l)}} \cdot X_{\text{Sn}} \tag{17}$$

The values of X_{SnO} and X_{Sn} are calculated from the compositions of slag and metal given in Table 2. Therefore, $\gamma_{\text{SnO(l)}}$ can be obtained by Eq. (18).

$$\log \gamma_{\text{SnO(l)}} = 13487/T - 4.026 + 1/2 \log P_{\text{O2}} - \log X_{\text{SnO}} + \log a_{\text{Sn(l)}} \tag{18}$$

The value of $a_{\text{Sn(l)}}$ in Pb–Sn melt has been reported at 1173 K by Goto and Pierre [44], as shown by data points and a broken line in Fig. 3. By applying a regular solution approximation to their $\gamma_{\text{Sn(l)}}$ value, that at T is derived by Eq. (19).

$$\log \gamma_{\text{Sn(l) at } T\text{[K]}} = 1173/T \cdot \log \gamma_{\text{Sn(l) at 1173 K}} \tag{19}$$

The Sn activity in Pb–Sn melt at 1573 K is shown by a solid line in Fig. 3.

Since Pb–Sn liquid was equilibrated with the molten slag containing SnO, PbO, and Fe_tO in a pure Fe crucible, the activity coefficients of PbO and Fe_tO can also be obtained.

The Pb(l)/PbO(l) equilibrium is written by Eq. (20) [41].

$$\text{Pb(l)} + 1/2\ \text{O}_2\text{(g)} = \text{PbO(l)} \tag{20}$$

$$\Delta G^{\circ}_{(20)} = -184440 + 69.79\,T\ \text{[Joule]}\ (1159 - 1897\ \text{K}) \tag{21}$$

From $\Delta G^{\circ}_{(20)}$, $\gamma_{\text{PbO(l)}}$ can be obtained by Eq. (22).

$$\log \gamma_{\text{PbO(l)}} = 9635/T - 3.646 + 1/2 \log P_{\text{O2}} - \log X_{\text{PbO}} + \log \gamma_{\text{Pb(l)}} + \log X_{\text{Pb}} \tag{22}$$

The Pb–Sn metal phase in this study contains a small amount of Sn, as shown in Table 2. Therefore, it is possible to assume $\gamma_{\text{Pb(l)}} = 1$ by applying Raoul's Law. From $\Delta G^{\circ}_{(6)}$, $\gamma_{\text{FetO(s)}}$ can be calculated by Eq. (23).

$$\log \gamma_{\text{FetO(s)}} = 13808/T - 3.381 + 1/2 \log P_{\text{O2}} - \log X_{\text{FetO}} \tag{23}$$

Figure 4 shows the activity coefficients of SnO, PbO, and Fe_tO of $CaO–SiO_2–Fe_tO$ slags with $RF = 0.51$ to 0.52 at 1573 K plotted against the C/S value. The activity coefficients of PbO and Fe_tO increased with the C/S value. On the other hand, SnO increased up to $C/S = 0.7$ but remained constant above it. Kudo et al. [37] reported that the PbO activity coefficient at 1573 K increased with C/S in the same slag system saturated with Fe. The trend shown in Fig. 4

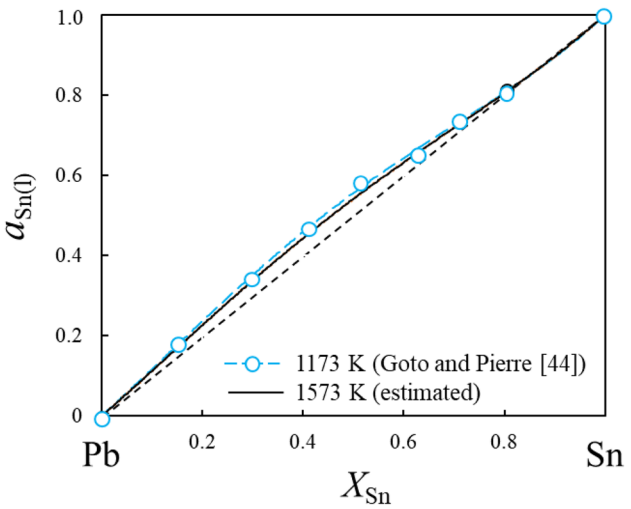

Fig. 3 Activity of Sn in Pb–Sn liquid at 1573 K plotted against X_{Sn}

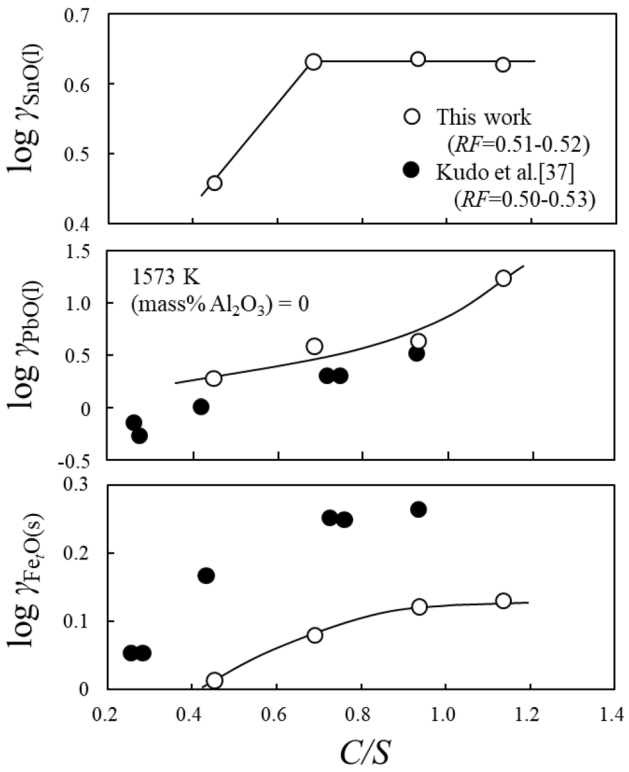

Fig. 4 The relationships between $\gamma_{\text{SnO(l)}}$, $\gamma_{\text{PbO(l)}}$, $\gamma_{\text{FetO(s)}}$, and C/S at 1573 K

is consistent with it. It can be said that the higher basicity, the easier SnO, PbO, and Fe_tO contained in the slag are reduced. Higher $\gamma_{SnO(l)}$ and $\gamma_{PbO(l)}$ are necessary to distribute Sn and Pb in the metal phase, while lower $\gamma_{Fe_tO(s)}$ to prevent FeO reduction. Therefore, a *C/S* value around 0.7 might be appropriate from Fig. 4.

It can be seen from Fig. 4 that the present $\gamma_{PbO(l)}$ and $\gamma_{Fe_tO(s)}$ values are different from those estimated using the data reported by Kudo et al. [37] The major difference in experimental methods is that they used ZrO_2–MgO solid electrolyte to measure the oxygen potential of the system, whereas CO–CO_2 mixed gas was used to determine the oxygen potential in this study. There may be other causes, but the reason for those differences of $\gamma_{PbO(l)}$ and $\gamma_{Fe_tO(s)}$ is not clear from this study, so it will be a subject of future investigation.

To obtain the Fe_tO concentration that favors SnO reduction, some experiments have been performed with varying the *RF* value, as described in (II) of Sect. "Slag Preparation". The activity coefficients of SnO, PbO, and FeO in the slag with *C/S* = 0.41 to 0.47 at 1573 K are plotted against *RF* value in Fig. 5. It is found that those activity coefficients increase with *RF* value. According to Eq. (10), a decrease in Fe_tO concentration corresponds to that in P_{O2}. Therefore, this trend suggests that SnO and PbO become difficult to be reduced as P_{O2} decreases in the reduction process, although such phenomena in actual operation had not been reported. Conversely, the activity coefficients of PbO and SnO become higher with Fe_tO concentration, so it can be said that the higher Fe_tO concentration is, the easier SnO and PbO reduction becomes. For comparison, the activity coefficients of PbO and FeO at 1573 K obtained by Kudo et al. [37], whose slag was also a CaO–SiO_2–Fe_tO system with *C/S* = 0.42 to 0.45, are plotted against *RF* value by closed circles in the same figure. Their trend, similar to this study, is observed in the relations between $\gamma_{PbO(l)}$ and *RF*, but their $\gamma_{Fe_tO(s)}$ becomes almost constant at high *RF*. The reason for the different trends in $\gamma_{PbO(l)}$ and $\gamma_{FeO(s)}$ is thought to be that the slag in this study contained SnO, but currently under investigation.

Finally, to investigate the effect of alumina addition on the activity coefficients of SnO, PbO, and FeO in slags was investigated using CaO–SiO_2–Fe_tO slag containing 5 to 15 mass% Al_2O_3. The activity coefficients of SnO, PbO, and Fe_tO in the slags with *C/S* = 0.45 to 0.50 and *RF* = 0.49–0.51 at 1573 K are plotted against the mole fraction of alumina, X_{Al2O3}, in Fig. 6. They tend to decrease with increasing X_{Al2O3}. Therefore, it is suggested that a lower alumina concentration is advantageous for SnO and PbO reduction.

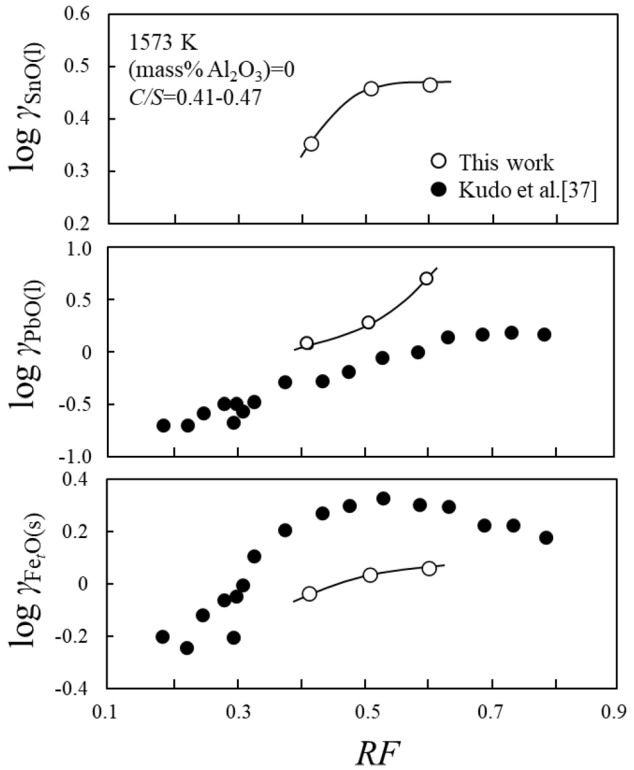

Fig. 5 The relationships between $\gamma_{SnO(l)}$, $\gamma_{PbO(l)}$, $\gamma_{Fe_tO(s)}$, and *RF* at 1573 K

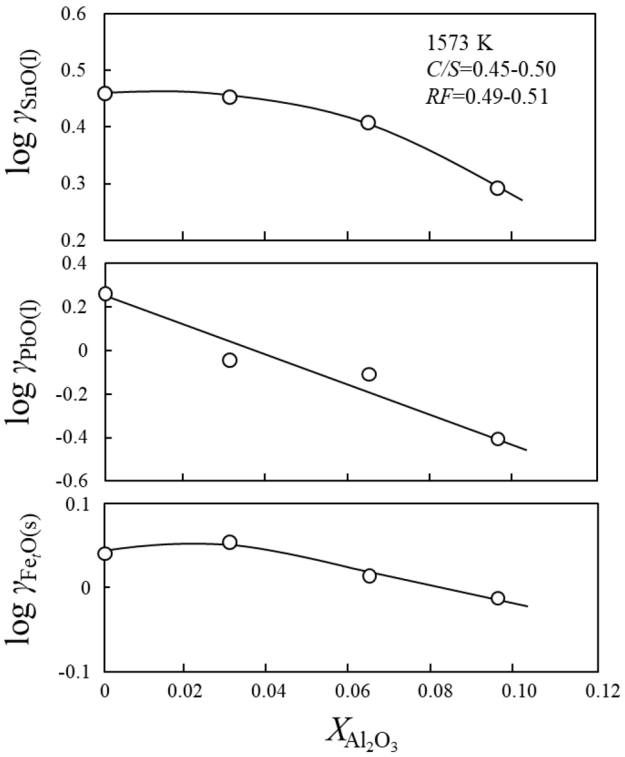

Fig. 6 The relationships between $\gamma_{SnO(l)}$, $\gamma_{PbO(l)}$, $\gamma_{Fe_tO(s)}$, and X_{Al2O3} at 1573 K

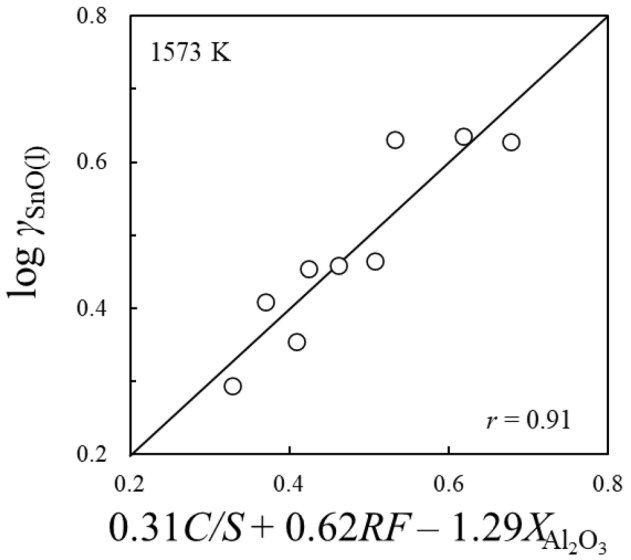

Fig. 7 The relation between the activity coefficient of SnO(l) obtained by Eq. (18) and calculated by Eq. (25)

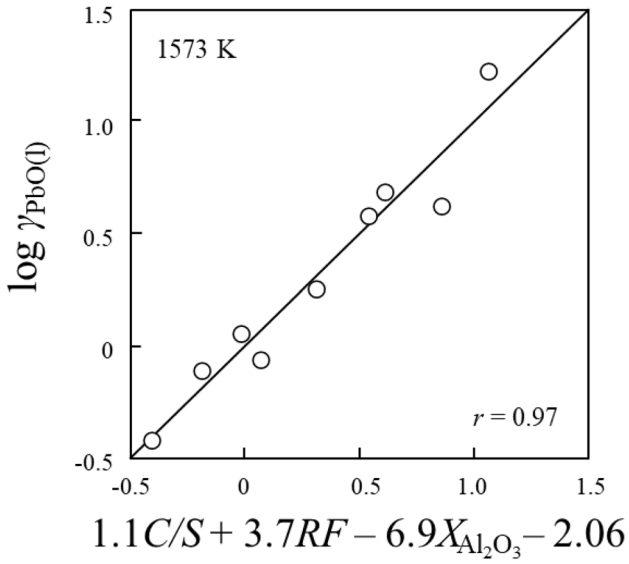

Fig. 8 The relation between the activity coefficient of PbO(l) obtained by Eq. (22) and calculated by Eq. (25)

Although the slag composition range in this study is narrow, an empirical equation was derived by multiple regression analysis for the effects of *C/S*, *RF,* and X_{Al2O3} on each activity coefficient. They are represented by Eqs. (24) to (26), where *r* is the correlation coefficient.

$$\log \gamma_{SnO(l)} = 0.31C/S + 0.62RF - 1.29X_{Al2O3} + 0.004 \, (r = 0.912) \quad (24)$$

$$\log \gamma_{PbO(l)} = 1.07C/S + 3.69RF - 6.86X_{Al2O3} - 2.062 \, (r = 0.970) \quad (25)$$

$$\log \gamma_{FetO(s)} = 0.37C/S + 0.62RF - 0.35X_{Al2O3} - 0.444 \, (r = 0.973) \quad (26)$$

The relations between the activity coefficients obtained by Eqs. (18), (22), and (23) and those calculated by Eqs. (24) to (26) are shown in Figs. 7, 8 and 9, respectively. Both are considered to be in good agreement from each figure and correlation coefficient. It is clear from these equations that *C/S* and *RF* affect positively and Al_2O_3 concentration negatively on the activity coefficients of SnO, PbO, and Fe_tO. From the coefficients of each function, the factor that most affects the activity coefficient is Al_2O_3 concentration for $\gamma_{SnO(l)}$, $\gamma_{PbO(l)}$, and *RF* for $\gamma_{FetO(s)}$. These trends can be explained by the following characteristics and interactions: In the experimental composition range of slag, it is considered that Sn, Pb and Fe behave as basic elements and Al behaves as an acidic element. Focusing on the variables in the regression equation, *C/S* and *RF* are related to slag basicity, and X_{Al2O3} to slag acidity. Therefore, the basic elements such as Sn, Pb and Fe are repelled under a more basic slag and attracted under a more acidic slag. Comparing three variables, Pb seems to be the most basic element from the coefficients of the regression equation.

Preferential Reduction of SnO and PbO

For the efficient recovery of valuable metals such as Sn and Pb in Cu recycling, it is important to suppress the FeO reduction as much as possible to prevent the Fe transfer to the metal phase.

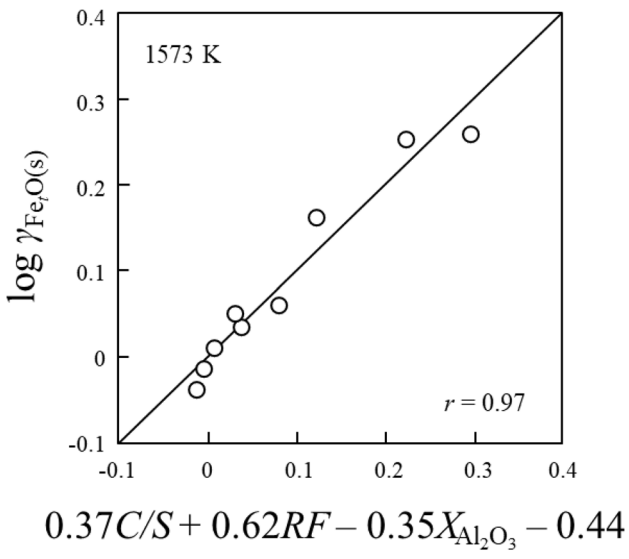

Fig. 9 The relation between the activity coefficient of $Fe_tO(s)$ obtained by Eq. (23) and calculated by Eq. (26)

The equilibrium reaction of Sn/SnO/Fe/Fe_tO is indicated by Eq. (27), whose $\Delta G^{\circ}_{(27)}$ is calculated by $\Delta G^{\circ}_{(6)}$ and $\Delta G^{\circ}_{(14)}$.

$$Sn(l) + Fe_tO(s) = SnO(l) + Fe(s) \quad (27)$$

$$\Delta G^{\circ}_{(27)} = \Delta G^{\circ}_{(14)} - \Delta G^{\circ}_{(6)} = 6135 + 12.35\,T\,[\text{Joule}] \quad (28)$$

$$= -RT\ln\left\{\left(\gamma_{SnO(l)} \cdot X_{SnO} \cdot a_{Fe(s)}\right)/\left(a_{Sn(l)} \cdot \gamma_{FetO(s)} \cdot X_{FetO}\right)\right\} \quad (29)$$

The relation between the distribution ratio of Sn between metal and slag, $a_{Sn(l)}/X_{SnO}$, and that of Fe, $a_{Fe(s)}/X_{FetO}$, at 1573 K is represented by Eq. (30) using Eqs. (24), (26) and (29), and shown in Fig. 10 as functions of *C/S* and X_{Al2O3}, whose variation range is 0.4–1.2 and 0–0.1, respectively, from Figs. 4 and 6.

$$\log\left(a_{Sn(l)}/X_{SnO}\right) = \log\left(a_{Fe(s)}/X_{FetO}\right) + 1.296 - 0.06C/S - 0.94X_{Al2O3} \quad (30)$$

Comparing $a_{Sn(l)}/X_{SnO}$ values at the same $a_{Fe(s)}/X_{FetO}$ value, $a_{Sn(l)}/X_{SnO}$ decreases with increasing *C/S* and X_{Al2O3}. However, since $a_{Sn(l)}/X_{SnO}$ value is much larger than $a_{Fe(s)}/X_{FetO}$ value, it can be said that Sn moves more easily from slag to metal than Fe.

From $\Delta G^{\circ}_{(31)}$ of Eq. (31), which is the equilibrium reaction of Pb/PbO/Fe/Fe_tO, the relation between the distribution ratio of Pb between metal and slag, $a_{Pb(l)}/X_{PbO}$, and that of Fe, $a_{Fe(s)}/X_{FetO}$, at 1573 K is represented by (34) using Eqs. (25), (26) and (33), and shown in Fig. 11 as functions of *C/S*, *RF,* and X_{Al2O3}.

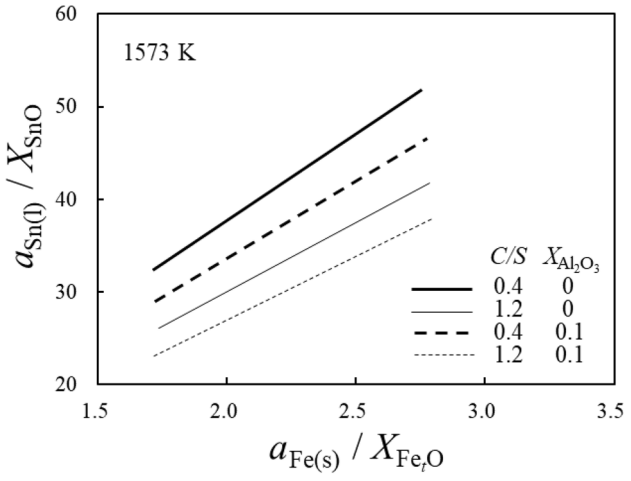

Fig. 10 Relationships between the distribution ratio of Sn between metal and slag and that of Fe at 1573 K as functions of *C/S* and X_{Al2O3}

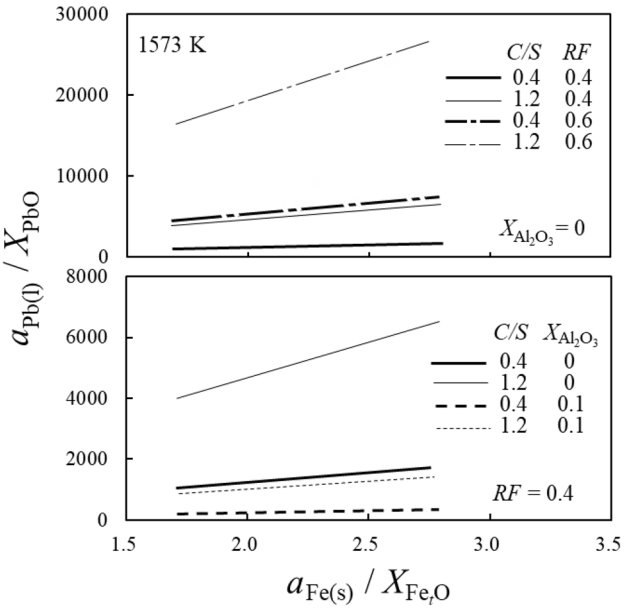

Fig. 11 Relationships between the distribution ratio of Pb between metal and slag and that of Fe at 1573 K as functions of *C/S*, *RF,* and X_{Al2O3}

$$Pb(l) + Fe_tO(s) = PbO(l) + Fe(s) \quad (31)$$

$$\Delta G^{\circ}_{(31)} = \Delta G^{\circ}_{(18)} - \Delta G^{\circ}_{(6)} = 79890 + 5.06\,T\,[\text{Joule}] \quad (32)$$

$$= -RT\ln\left\{\left(\gamma_{PbO(l)} \cdot X_{PbO} \cdot a_{Fe(s)}\right)/\left(a_{Pb(l)} \cdot \gamma_{FetO(s)} \cdot X_{FetO}\right)\right\} \quad (33)$$

$$\log\left(a_{Pb(l)}/X_{PbO}\right) = \log\left(a_{Fe(s)}/X_{FetO}\right) + 1.299 + 0.70C/S + 3.08RF - 6.51X_{Al2O3} \quad (34)$$

When comparing $a_{Pb(l)}/X_{PbO}$ values at the same $a_{Fe(s)}/X_{FetO}$ value, $a_{Pb(l)}/X_{PbO}$ increases with *C/S* and *RF*, while that decreased with increasing X_{Al2O3}. However, since $a_{Pb(l)}/X_{PbO}$ value is extremely larger than both $a_{Sn(l)}/X_{SnO}$ and $a_{Fe(s)}/X_{FetO}$ values, it is expected that PbO is reduced more easily than SnO and Fe_tO.

In this study, the slag composition suitable for reducing SnO and PbO was thermodynamically discussed using activity coefficients. However, in practical operation, in addition to the equilibrium reduction degree of target oxides, their mass transfer rates in the slag, which are affected by slag viscosity, also influence the reduction rate. The relationship between SnO reduction rate and slag viscosity will be reported in a separate paper.

Conclusions

Activity coefficients of SnO, PbO, and Fe_tO in $CaO–SiO_2–Fe_tO–Al_2O_3$ slag were determined at 1573 K with varying slag basicities and the concentrations of Fe_tO and Al_2O_3. The results obtained can be summarized as follows.

(1) The activity coefficients of PbO and Fe_tO increased with the *C/S* value. On the other hand, SnO increased to $C/S = 0.7$ but remained constant above it.
(2) The activity coefficients of SnO, PbO, and Fe_tO increased with increasing Fe_tO concentration and decreasing Al_2O_3 concentration.
(3) The activity coefficients were represented by the following empirical equations.

$$\log \gamma_{SnO(l)} = 0.31C/S + 0.62RF - 1.29X_{Al2O3} + 0.004$$

$$\log \gamma_{PbO(l)} = 1.07C/S + 3.69RF - 6.86X_{Al2O3} - 2.062$$

$$\log \gamma_{FetO(s)} = 0.37C/S + 0.62RF - 0.35X_{Al2O3} - 0.444$$

(4) The order of reducibility was $PbO > SnO >> Fe_tO$ when comparing $a_{Sn(l)}/X_{SnO}$, $a_{Pb(l)}/X_{PbO}$ and $a_{Fe(s)}/X_{FetO}$.
(5) The slag condition favorable to SnO and PbO reduction is higher basicity, around 50 mass% Fe_tO, and lower Al_2O_3 content.

It is expected that this slag composition can help optimizing the WEEE recycling process in the Sn and Pb recovery from the slag.

Acknowledgements The authors sincerely appreciate the partial financial support from Dowa Metals & Mining Co. Ltd.

Conflict of interest On behalf of all authors, the corresponding author states that there is no conflict of interest.

References

1. Olivetti EA, Cullen JM (2018) Toward a sustainable materials system. Science 360:1396–1398. https://doi.org/10.1126/science.aat6821
2. Halada K, Shimada M, Ijima K (2008) Forecasting of the consumption of metals up to 2050. Mater Trans 49:402–410. https://doi.org/10.2320/matertrans.ML200704
3. Halada K (2020) Activities of circular economy in japan—towards global multi-value circulation. Int J Autom Technol 14:867–872. https://doi.org/10.20965/ijat.2020.p0867
4. Schmid M (2019) Mitigating supply risks through involvement in rare earth projects: Japan's strategies and what the US can learn. Resour Policy 63:101457. https://doi.org/10.1016/j.resourpol.2019.101457
5. Mancheri NA, Sprecher B, Bailey G et al (2019) Effect of Chinese policies on rare earth supply chain resilience. Resour Conserv Recycl 142:101–112. https://doi.org/10.1016/j.resconrec.2018.11.017
6. Mancheri NA (2015) World trade in rare earths, Chinese export restrictions, and implications. Resour Policy 46:262–271. https://doi.org/10.1016/j.resourpol.2015.10.009
7. Raabe D, Tasan CC, Olivetti EA (2019) Strategies for improving the sustainability of structural metals. Nature 575:64–74. https://doi.org/10.1038/s41586-019-1702-5
8. Kato Y, Koyama M, Fukushima Y et al (2016) Energy technology roadmaps of Japan. Springer, Tokyo
9. Baba Y, Kubota F, Kamiya N, Goto M (2011) Recent advances in extraction and separation of rare-earth metals using ionic liquids. J Chem Eng Jpn 44:679–685. https://doi.org/10.1252/jcej.10we279
10. Yamasue E, Minamino R, Numata T et al (2009) Novel evaluation method of elemental recyclability from urban mine-concept of urban ore TMR. Mater Trans 50:1536–1540. https://doi.org/10.2320/matertrans.MBW200816
11. Tejaswini MSSR, Pathak P, Gupta DK (2022) Sustainable approach for valorization of solid wastes as a secondary resource through urban mining. J Environ Manage 319:115727. https://doi.org/10.1016/j.jenvman.2022.115727
12. Arora R, Paterok K, Banerjee A, Saluja MS (2017) Potential and relevance of urban mining in the context of sustainable cities. IIMB Manage Rev 29:210–224. https://doi.org/10.1016/j.iimb.2017.06.001
13. Brunner PH (2011) Urban mining a contribution to reindustrializing the city. J Ind Ecol 15:339–341. https://doi.org/10.1111/j.1530-9290.2011.00345.x
14. Avarmaa K, Klemettinen L, O'Brien H, Taskinen P (2019) Urban mining of precious metals via oxidizing copper smelting. Miner Eng 133:95–102. https://doi.org/10.1016/j.mineng.2019.01.006
15. Jones PT, Geysen D, Tielemans Y et al (2013) Enhanced landfill mining in view of multiple resource recovery: a critical review. J Clean Prod 55:45–55. https://doi.org/10.1016/j.jclepro.2012.05.021
16. Sum EYL (1991) The recovery of metals from electronic scrap. JOM 43:53–61. https://doi.org/10.1007/BF03220549
17. Sakamura Y, Hijikata T, Kinoshita K et al (1998) Measurement of standard potentials of actinides (U, Np, Pu, Am) in LiCl-KCl eutectic salt and separation of actinides from rare earths by electrorefining. J Alloys Compd 271–273:592–596. https://doi.org/10.1016/S0925-8388(98)00166-2
18. Barakat MA (1998) Recovery of lead, tin and indium from alloy wire scrap. Hydrometallurgy 49:63–73. https://doi.org/10.1016/s0304-386x(98)00003-6
19. Van den Bulck A, Turner S, Guo M et al (2018) The distribution of Sn between $CaO–CuO_x–FeO_y–SiO_2$ slag and copper metal at

1300 °C. Proc Extr 2018:1083–1092. https://doi.org/10.1007/978-3-319-95022-8_87
20. Nakamura T (2018) Smelting technologies for E-scrap in Japan. Review of printed circuit board recycling processes. Workshop 2018 of the Asian Network for Prevention illegal Transboundary Movement of Hazardous Wastes. Akita, Japan. https://www.env.go.jp/en/recycle/asian_net/Annual_Workshops/2018_PDF/Day2_KeynoteLecture/22Day2_KL_01_ANWS2018.pdf. Accessed 20 July 2023
21. Lennartsson A, Engström F et al (2018) Large-scale WEEE recyclng integrated in an ore-based Cu-extraction system. J Sustain Metall 4:222–232. https://doi.org/10.1007/s40831-018-0157-5
22. Rankin WJ (1986) The slag-metal equilibrium in tin smelting. Metall Trans B 17:61–68. https://doi.org/10.1007/BF02670819
23. Xu X, Hayes PC, Jak E (2013) Experimental study of phase equilibria in the "SnO"-CaO-SiO_2 system in equilibrium with tin metal. Int J Mater Res 104:235–243. https://doi.org/10.3139/146.110865
24. Shevchenko M, Ilyushechkin A, Abdeyazdan H, Jak E (2021) Integrated experimental phase equilibria study and thermodynamic modeling of the PbO–SnO–SnO_2–SiO_2 system in air and in equilibrium with Pb–Sn metal. J Alloys Compd 888:161402. https://doi.org/10.1016/j.jallcom.2021.161402
25. Shishin D, Hidayat T, Sultana U et al (2020) Experimental measurement and thermodynamic model predictions of the distributions of Cu, As, Sb and Sn between liquid lead and PbO–FeO–Fe_2O_3–SiO_2 slag. Int J Mater Res 111:733–743. https://doi.org/10.3139/146.111942
26. Karakaya I, Thompson WT (1988) The Pb-Sn (lead-tin) system. J Phase Equilib 9:144–152. https://doi.org/10.1007/BF02890552
27. Das SK, Ghosh A (1972) Thermodynamic measurements in molten Pb-Sn alloys. Metall Trans 3:803–806. https://doi.org/10.1007/bf02647652
28. Ngai TL, Chang YA (1981) A thermodynamic analysis of the Pd-Sn system and the calculation of the Pb-Sn phase diagram. Calphad 5:267–276. https://doi.org/10.1016/0364-5916(81)90009-2
29. Takeda Y, Yazawa A, Chit PP, Ujiie H (1990) Equilibria between liquid tin and FeO_x-CaO-SiO_2 slag. Mater Trans JIM 31:793–801. https://doi.org/10.2320/matertrans1989.31.793
30. Yamaguchi K, Ueda S, Takeda Y (2005) Phase equilibrium and thermodynamic properties of SiO_2-CaO-FeO_x slags for copper smelting-research achievements of Professor Yoichi Takeda. Scand J Metall 34:164–174. https://doi.org/10.1111/j.1600-0692.2005.00737.x
31. Buchmann M, Borowski N et al (2020) Evaluation of recyclability of a WEEE slag by means of integrative X-ray computer tomography and SEM-based image analysis. Minerals 10:309–327. https://doi.org/10.3390/min10040309
32. Takeda Y, Ishiwata S, Yazawa A (1983) Distribution equilibria of minor elements between liquid copper and calcium ferrite slag. Trans Jpn Inst Met 24:518–528. https://doi.org/10.2320/matertrans1960.24.518
33. Anindya A, Swinbourne DR et al (2013) Distribution of elements between copper and FeO_x-CaO-SiO_2 slags during pyrometallurgical processing of WEEE part 1-tin. Miner Process Extr Metall 122:165–173
34. Nagamori M, Mackey PJ (1977) Distribution equilibria of Sn, Se and Te between FeO-Fe_2O_3-SiO_2-Al_2O_3-$CuO_{0.5}$ slag and metallic copper. Metall Trans B 8:39–46. https://doi.org/10.1007/BF02656349
35. Alcock CB, Sridhar R, Svedberg RC (1969) A mass spectrometric study of the binary liquid alloys, Ag-In and Cu-Sn. Acta Metall 17:839–844. https://doi.org/10.1016/0001-6160(69)90103-5
36. Ralph H, Pramod D (1971) Selected thermodynamic values and phase diagrams for copper and some of its binary alloys. International Copper Research Association, Washington, DC
37. Kudo M, Jak E, Hayes P et al (2000) Lead solubility in FeO_x-CaO-SiO_2 slags at iron saturation. Metall Mater Trans B 31:15–24. https://doi.org/10.1007/s11663-000-0126-8
38. FactSage 8.1. https://www.factsage.com. Accessed 07 Feb 2022
39. Chen M, Avarmaa K et al (2021) Handling trace element in WEEE recycling through copper smelting-an experimental and thermodynamic study. Miner Eng 173:107189–107202. https://doi.org/10.1016/j.mineng.2021.107189
40. Kato M, Iwama T, Inoue R et al (2022) CAMP-ISIJ. 35 1:CD-ROM. (**in Japanese**)
41. Knacke O, Kubaschewski O, Hesselmann K (1991) Thermochemical properties of inorganic substances, 2nd edn. Springer-Verlag, Verlag Stahleisen Gmbh, Berlin, Germany
42. Stull DR, Prophet H (1971) JANAF Thermochemical tables, 2nd edn. National Bureau of Standards, Gaithersburg
43. Kuxmann U, Dobner R (1980) Study of the tin-tin (IV) oxide system in the miscibility temperature region. Metall 34:821
44. Goto K, St Pierre G (1963) Measurement of chemical activities in lead-tin binary liquid solution. Tetsu-to-Hagané 49:1873–1879. https://doi.org/10.2355/tetsutohagane1955.49.13_1873